Solid State Communications 181 (2014) 54–59

Contents lists available at ScienceDirect

Solid State Communications

journal homepage: www.elsevier.com/locate/ssc

Lattice dynamics and superconducting properties of antiperovskite La_3InZ (Z=N,O)

Swetarekha Ram, V. Kanchana *

Department of Physics, Indian Institute of Technology Hyderabad, Ordnance Factory Estate, Yeddumailaram 502 205, Andhra Pradesh, India

ARTICLE INFO

Article history:
Received 19 August 2013
Received in revised form
11 November 2013
Accepted 19 November 2013
by E.V. Sampathkumaran
Available online 4 December 2013

Keywords:
A. Superconductor
D. Electron–phonon interactions
D. Electronic band structure
D. Phonon

ABSTRACT

Electronic and superconducting properties of La_3InZ (Z=N, O) compounds are studied and are compared with La_3In. From the density of states of La_3InZ it is quite clear that the hybridization between La-*d* and In-*p* states gets reduced with the inclusion of the Z atom in comparison with La_3In. A Fermi surface topology change is observed only in La_3InO under compression, which is attributed to the non-monotonic variation of the density of states. The calculated superconducting transition temperature (T_c) is less than 2 K for N containing compound, and is found to be above 2 K for O containing compound and the trend agrees well with the experimental findings. The reason for the suppression of the T_c due to the inclusion of the Z atom is also discussed from the band structure and phonon dispersion plots, where we find the phonon modes to harden in La_3InZ.

1. Introduction

Over the past decade the binary intermetallic alloys of AX_3 and A_3X (A=La, X=Sn, In, Tl) type have been widely investigated which are found to be superconductors and the reported superconducting transition temperature (T_c) is found to be highest around 10 K in La_3In [1]. It is quite interesting to study the superconducting properties of La_3InZ compounds formed by addition of the Z (N, O) atom to La_3In yet remaining in the same space group. Earlier studies report an enhancement of the T_c by addition of carbon in YNi_4B [2], whereas the decrease in T_c was reported by addition of carbon in La_3X (X=Al, Ga, In, Tl) compounds [3]. The presence of superconductivity in the La–Ca–Cu–O compound was reported under high oxygen pressure, whereas the superconductivity was found to vanish under low oxygen pressure [4]. Apart from this the reduction of T_c was also reported in MgB_2 by carbon doping [5]. Again from experimental study on the superconducting behavior of La_3InZ (Z=N, O) [6], it is to be noted that La_3In and La_3InO have T_c of the same range around 10 K, which further motivate us to study the role of Z in La_3InZ compounds. In this present study, we calculate the superconducting transition temperature of these compounds and show the presence of superconductivity below 2 K for La_3InN and above 2 K in the case of La_3InO at ambient temperature. In addition, we also bring out the role of Z in the superconducting properties of La_3InZ compounds. Experimentally Zhao et al. [6] have synthesized these compounds and reported the superconducting behavior at nearly 10 K for La_3InO, whereas the authors have not found any superconducting nature in La_3InN above 2 K. In addition Kirchner et al. [7] have studied experimentally as well as theoretically a series of $(R_3N)In$ (R=La–Nd, Lu, Sm–Tm) compounds and compared the bonding nature of La_3InN with La_3In theoretically. Apart from this no theoretical studies are available regarding the band structure, density of states, Fermi surface at ambient pressure as well as under compression. The rest of the paper is organized as follows: in the next section, we briefly discuss the computational details, results and discussions presented in Section 3, which contains electronic, Fermi surface, superconducting properties of these compounds, finally we summarize and conclude our paper.

2. Computational details

The electronic structure calculations were performed using the full-potential linear augmented plane wave (FP-LAPW) method as implemented in the WIEN2k [8] based on the generalized gradient approximation of Perdew, Burke and Ernzerhof (GGA-PBE) [9]. For the total energy convergence $R_{MT}K_{max}=8$ was used, where R_{MT} is the smallest muffin-tin radius, and K_{max} is the plane wave cut-off. The charge density was Fourier expanded up to $G_{max}=12$ a.u.$^{-1}$. The muffin-tin radii were chosen as 2.5 a.u. for La, 2.3 a.u. for In and 1.7 a.u. for Z (N, O) atoms. A $(44\times44\times44)$ *k*-point mesh in the Monkhorst–Pack [10] scheme was used during the self-consistent

* Corresponding author. Tel.: +91 40 23016019.
E-mail addresses: kanchana.vaithee@gmail.com, kanchana@iith.ac.in (V. Kanchana).

0038-1098/$ - see front matter © 2013 Elsevier Ltd. All rights reserved.
http://dx.doi.org/10.1016/j.ssc.2013.11.032

cycle to ensure accurate determination of the Fermi level. The three dimensional (3D) Fermi surface plots were generated with the help of the Xcrysden molecular structure visualization program [11]. Spin-orbit coupling (SOC) is not included for all the electronic structure calculations as we find the vicinity of the Fermi level to remain unaltered with the inclusion of the SOC. We have used the experimental lattice constant of 5.11 Å and 5.19 Å, for La_3InN and La_3InO [6], respectively, and the corresponding experimental volumes are denoted by V_0 in the following.

For the electron–phonon coupling constant and the phonon dispersion plots, we have used the Quantum espresso package [12,13]. In order to deal with the possible convergence problem for metals, a smearing technique is employed using the Methfessel–Paxton (MP) scheme, with the smearing parameter set to 0.02 Ry for La_3InZ (Z=N, O) compounds. For the energy convergence we have used the wave function and charged-density cutoffs of 30 Ry and 320 Ry, respectively, for La_3InN and 56 Ry and 560 Ry, respectively, for La_3InO. Phonon calculations were carried out for $4\times4\times4$ Monkhorst–Pack q-point grid with Brillouin zone integrations on a $32\times32\times32$ mesh.

3. Results and discussion

3.1. Band structure, densities of states and Fermi surface

The calculated band structures of La_3InZ (Z=N, O) without spin orbit coupling at experimental volume (V_0) are presented in Fig. 1. The band structure plots reveal the overall profile of both the compounds to be similar except band filling in the case of La_3InO due to an extra electron in O, which is also clearly seen in the corresponding Fermi surface (FS) and the density of states (DOS) as shown in Figs. 2 and 3, respectively. From the FS plots we can see the three extra hole pockets centered at the R point in the case of the La_3InN, which is absent in La_3InO due to the positioning of the band below the Fermi level (see Fig. 2(a–c) and see solid black, broken red and dotted blue color band in Fig. 1). In addition we have an extra electron sheet along Γ–R direction in the case of La_3InO as shown in Fig. 2(h) (broken indigo color band in Fig. 1(b)). Apart from this the topology of the fourth FS of N containing compound (Fig. 2(d)) and the first FS of O (Fig. 2(f)) containing compound (see solid line with sphere magenta color band) are found to be similar except the increase in the width of the tube along the Γ–X direction and are having both electron as well as hole character. This is again evident from the band structure plots in Fig. 1 as we could see the same band to dip more below the Fermi level at X point in the case of La_3InO, resulting in wider opening along Γ–X. The fifth FS of N containing compound (Fig. 2(e)) and the second FS of O containing compound (Fig. 2(g)) are electron pocket centered at Γ, with size being larger in La_3InO than in La_3InN. If we compare the FS of the La_3In with La_3InZ (Z=N, O), we could find the FS topology of these compounds to be quite different as shown in Fig. 2 (the details of the calculation regarding La_3In can be found else where [14]) and it is interesting to analyze and to compare La_3In and La_3InO which are claimed experimentally to be a superconductor with T_c around 10 K, provoking us to study the role of O in this compound. To analyze in detail, we have plotted the density of states of La_3InZ along with La_3In as shown in Fig. 3. More interestingly we find the Fermi level of both La_3InO and La_3In to fall very close to the peak. But the density of states at the Fermi level ($N(E_F)$) was found to be higher in La_3In [15] ($N(E_F)=7.80$ states/eV) in comparison with La_3InO ($N(E_F)=$ 2.86 states/eV), which might eventually give an indication of the suppression of the T_c in La_3InO which will be discussed little later. Further analyzing the partial density of states of La_3InO from Fig. 3(a), we find the major contribution to stem from La-d along with the hybridization of the In-p and O-p states at the Fermi level. In addition we could also see the Fermi level (E_F) lying close to a peak in the case of La-d and O-p orbitals, whereas the E_F falls on pseudogap of In-p orbital. In contrast to La_3In, the E_F lies close to the peak for both La-d and In-p orbital and is well evident from Fig. 3(b). So the extent of hybridization of In-p with La-d is reduced in the case of La_3InO, whereas there exists a pronounced hybridization between La-d and O-p, which brings in the role of O in La_3InO. Next we turn our discussion towards comparing La_3InN and La_3InO. As we move from N to O, the band gets filled and is seen in the band structure and FS, which we have presented so far. Now if we compare these compounds from the projected density of states, we could see the Fermi level to fall exactly on the pseudogap in the case of La_3InN and it is clearly evident from the La-d and N-p states in Fig. 3(a). The extent of hybridization between La-d and In-p is again found to be lesser similar to La_3InO. A similar hybridization effect in La_3InN was also presented by Kirchner et al. [7], where the authors clearly show the metallic nature of this compound and the presence of the metal–metal bonding between La-d and In-p. Again the $N(E_F)$ for La_3InN is found to be 2.55 states/eV, which is also lesser than both La_3In and La_3InO indicating the T_c to be lesser in comparison with both La_3In and La_3InO. Our calculated $N(E_F)$ for La_3InN agrees well with the value reported by Kirchner et al. [7].

More interestingly we have observed a FS topology change under compression in the case of La_3InO, whereas the topology is found to remain unaltered under compression in La_3InN. In the case of La_3InO we find the first three surfaces to appear under compression around $V/V_0=0.8$ at R point similar to La_3InN (Fig. 2 (a–c)), due to the upward movement of the band and an extra electron pocket appears along the M–Γ direction in the last FS due to the downward shift of the band. This observed difference between La_3InN and La_3InO is mainly due to the non-monotonic variation of $N(E_F)$ only in La_3InO as shown in Fig. 3(b), whereas we

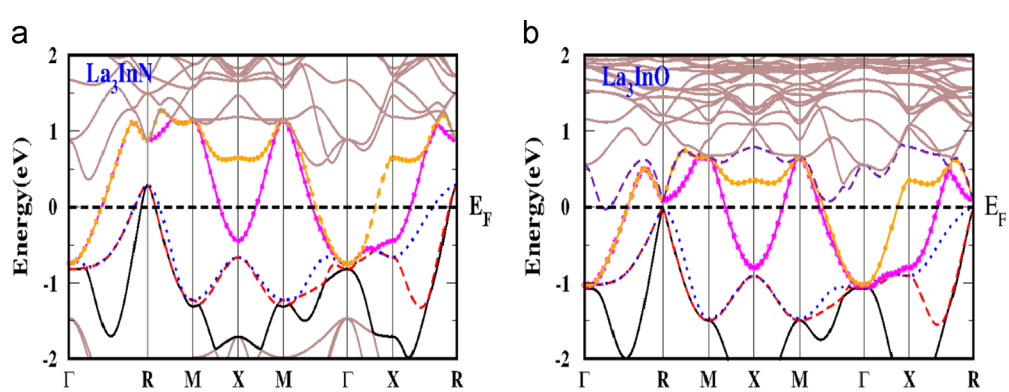

Fig. 1. (Color online) Band structure of La_3InZ (Z=N, O) at $V/V_0=1.0$. The bands crossing the Fermi level are shown in different colors.

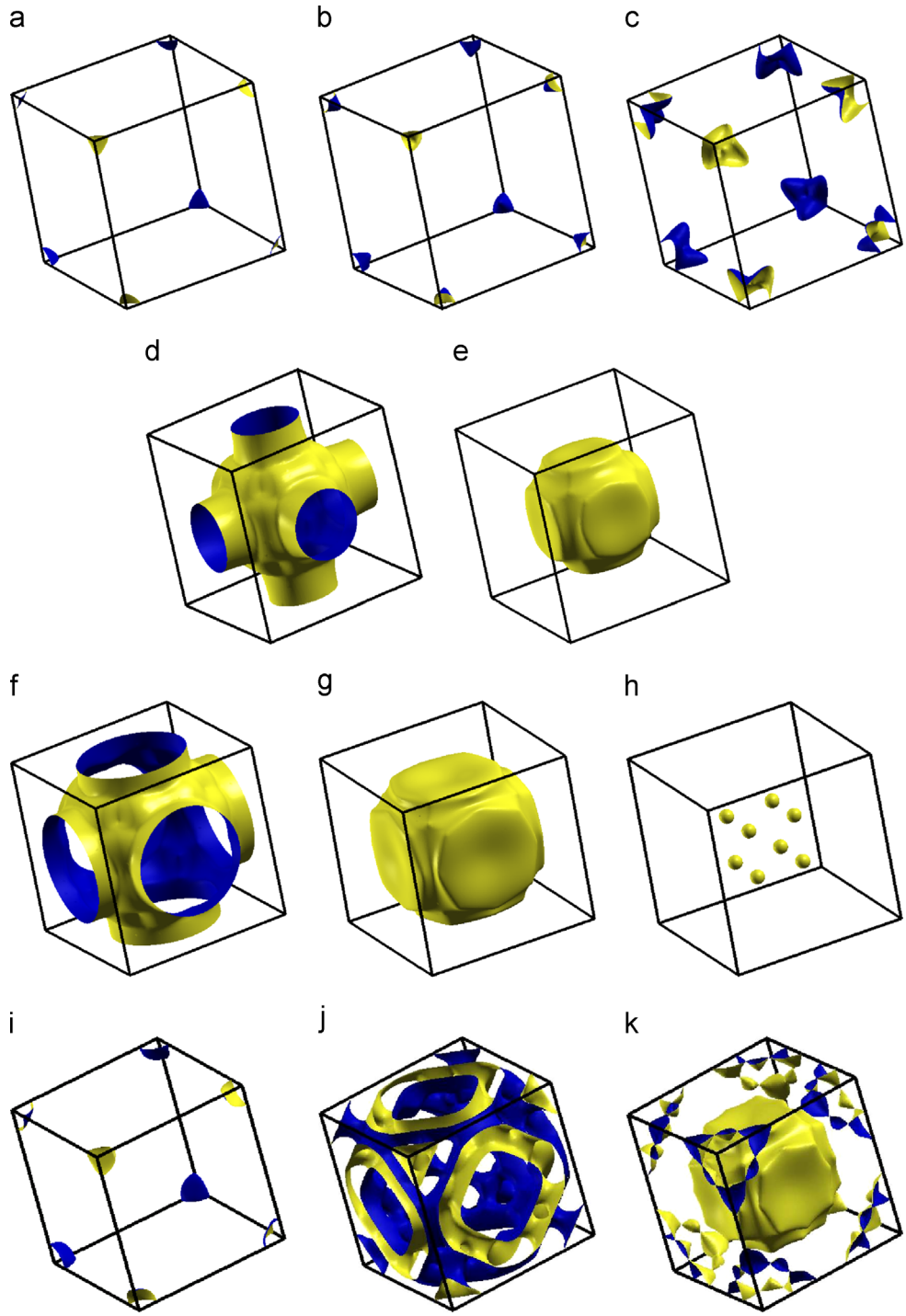

Fig. 2. (Color online) Fermi surface of La_3InZ (Z=N, O) and La_3In at $V/V_0=1.00$, first and second rows are the FS for La_3InN, third row is for La_3InO and the fourth row is for La_3In.

find the $N(E_F)$ to vary linearly with compression in the case of La_3InN. A similar scenario is also observed in our previous study for AX_3 (A=La, Y; X=In, Tl, Sn, Pb) series of compounds, where we have seen a non-monotonic variation of $N(E_F)$ eventually leading to a FS topology change [16]. In addition we can observe the sudden increase in density of states at $V/V_0=0.8$ in La_3InO where we have also found three extra hole pocket and an additional electron sheet in the last surface to appear. Overall we have seen the bands to move up for La_3InN under compression and in the case of La_3InO simultaneous upward and downward shift of the bands is observed.

3.2. Superconductivity and vibrational properties

From the $N(E_F)$, we may calculate the Sommerfeld coefficient of specific heat (γ), and the values are reported in Table 1. From the γ values one may expect T_c to be higher in La_3InO in comparison with La_3InN. From the Eliashberg function we have calculated the electron–phonon coupling constant λ_{ep}, and having calculated the λ_{ep} we estimate the T_c of both the compounds by using Allen–Dynes formula [17] and the values are reported in Table 1 along with the calculated $N(E_F)$. The dimensionless μ^*, the Coulomb pseudo-potential used in our calculation for all the compounds is

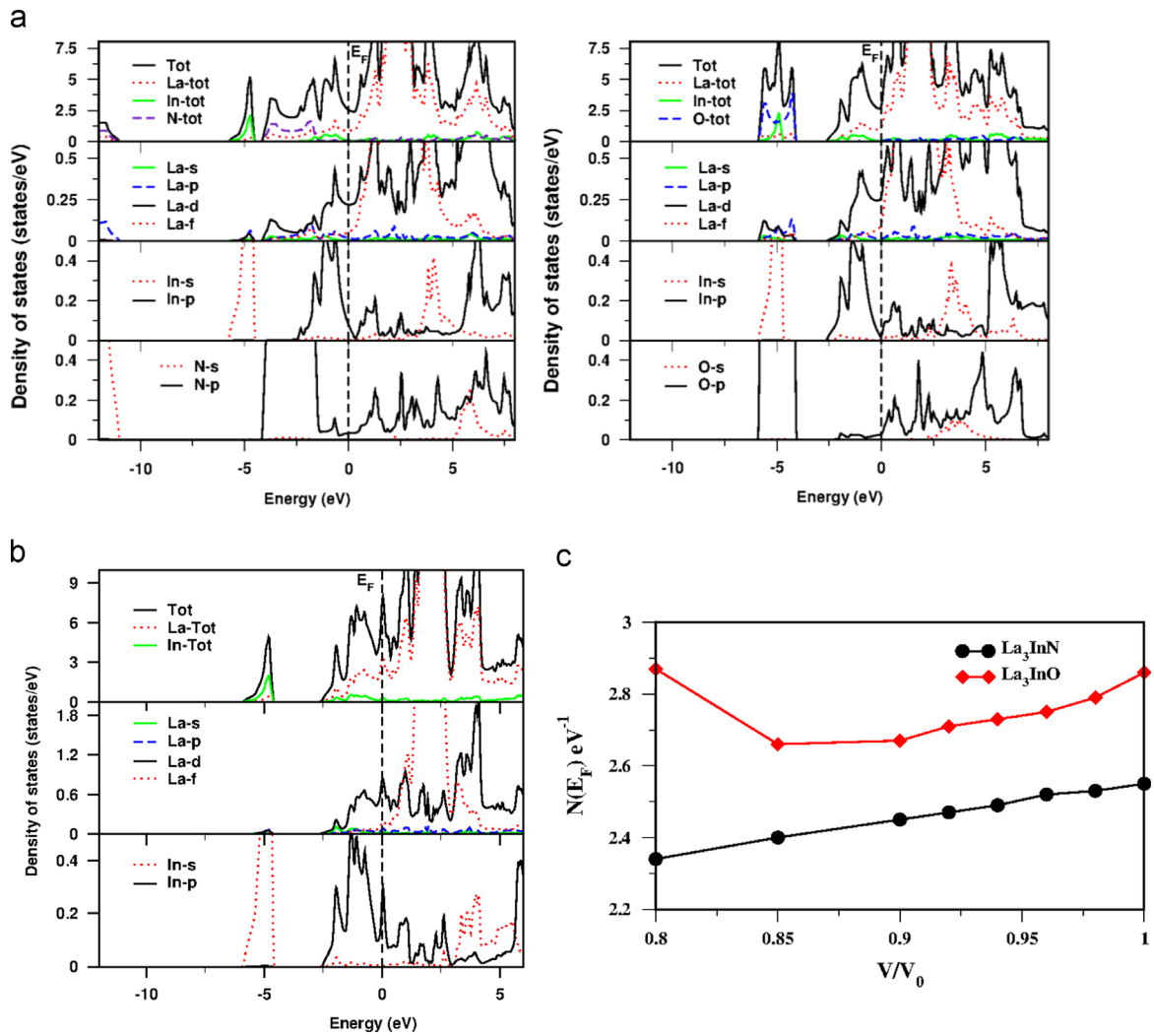

Fig. 3. (Color online) (a) Density of states at $V/V_0=1.0$ for La_3InZ (Z=N, O) and (b) the density of states for La_3In, (c) variation of $N(E_F)$ under compression for La_3InZ (Z=N, O).

Table 1
Calculated density of states at the Fermi level, $N(E_F)$ (in states per eV and per formula unit, evaluated at the experimental equilibrium volumes), together with derived Sommerfeld constants, γ, averaged phonon frequency, ω_{ln} the electron-phonon coupling constant, λ_{ep} and superconducting transition temperature, T_c for La_3InZ (Z=N, O) and La_3In.

Compounds		$N(E_F)$	γ (mJ/mol K^2)	ω_{ln} (cm^{-1})	λ_{ep}	T_c (K)
La_3InN	This work	2.55	6.02	107.97	0.37	0.44
	Others[a]	2.6				–
La_3InO	This work	2.86	6.74	98.29	0.62	3.77
	Expt.					10[b]
La_3In	This work	7.8	18.40	62.7	0.97	6.36

[a] Ref. [7].
[b] Ref. [6].

0.1. The calculated averaged phonon frequency ω_{ln} for both the compounds along with La_3In is also reported in Table 1.

From our calculated values we find T_c of La_3InO to be higher than La_3InN with higher electron–phonon coupling constant λ_{ep}, and find this trend to agree well with the calculated $N(E_F)$. Our calculated value of T_c is comparatively lesser when compared to the experimental value [6] in the case of La_3InO and this might be due to the polycrystalline or non-stoichiometric nature of the sample [18,19]. Unfortunately there are no other theoretical values available for comparing the results of these studied compounds, whereas the trend of our calculated T_c is the same as in Ref. [6], where the authors have reported T_c to below 2 K for La_3InN and above 2 K in the case of La_3InO. Again when we compare La_3In with the presently studied compounds we find the calculated T_c value of La_3In (T_c=6.36 K) to be higher in comparison with La_3InZ (Z=N, O), with higher electron–phonon coupling constant (λ_{ep}=0.97), as evident from the reported values in Table 1 and it contradicts the experimental finding where the authors have reported the T_c of La_3In and La_3InO to be the same [1,6] and we try to justify the same from the calculated phonon dispersion relations as discussed below.

We have plotted the phonon-dispersion along with the phonon density of states (PDOS) in Fig. 4 at ambient pressure for both the studied compounds La_3InN and La_3InO along with La_3In. From the figure we can see all the phonon modes to have positive frequency in all high symmetry directions, which ultimately gives the confirmation towards the dynamical stability of these compounds. Again we find the phonon frequency to be higher in La_3InN than in La_3InO. The lower mass in the case of the La_3InN may be the reason for the phonon mode to be higher in frequency when compared with La_3InO. In addition we have calculated the zone center phonon frequency as follow:

$$La_3InN = 3T_{1u}(0\ \text{cm}^{-1}) + 3T_{1u}(87.2\ \text{cm}^{-1}) + 3T_{2u}(87.4\ \text{cm}^{-1}) + 3T_{1u}(140.4\ \text{cm}^{-1}) + 3T_{1u}(298.2\ \text{cm}^{-1})$$

$$La_3InO = 3T_{1u}(0\ \text{cm}^{-1}) + 3T_{1u}(66.0\ \text{cm}^{-1}) + 3T_{2u}(97.0\ \text{cm}^{-1}) + 3T_{1u}(125.3\ \text{cm}^{-1}) + 3T_{1u}(274.2\ \text{cm}^{-1})$$

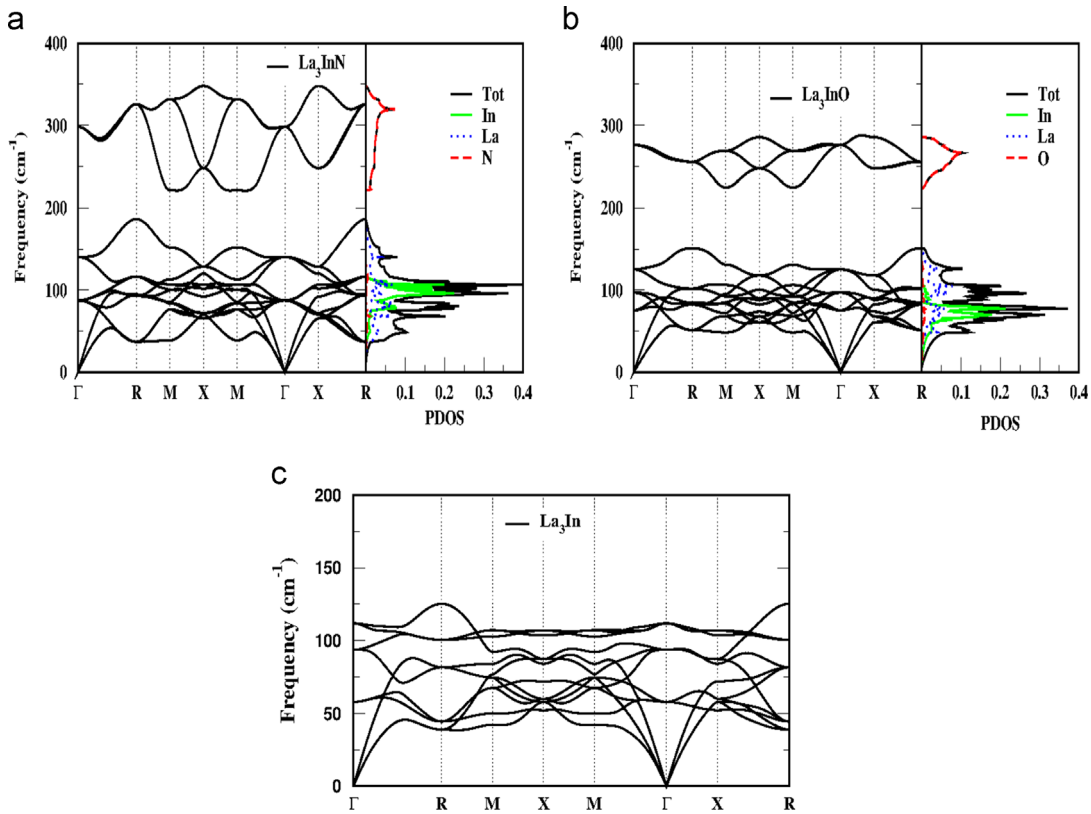

Fig. 4. (Color online) Phonon dispersion plots along with the phonon density of states for (a) La_3InN, (b) La_3InO and (c) is the dispersion for the La_3In at $V/V_0=1.0$.

$$La_3In = 3T_{1u}(0\ cm^{-1}) + 3T_{2u}(57.8\ cm^{-1}) + 3T_{1u}(94.8\ cm^{-1}) + 3T_{1u}(112.0\ cm^{-1})$$

If we compare La_3In and La_3InO, we find the phonon modes to soften in the case of La_3In in comparison with La_3InO. The hardening of the phonon modes in La_3InO might be reducing the electron–phonon coupling constant in the case of La_3InO in comparison with La_3In leading to the reduction in superconducting transition temperature of La_3InO. The hardening of the phonon modes is mainly due to the presence of the O atom and is well evident from the PDOS in Fig. 4, where we can see the contribution at higher frequency regions to arise mainly from the O atom. Again when we move to La_3InN and compare with La_3InO, we could see all the phonon modes except the T_{2u} mode to soften in the case of La_3InO. The softening of the T_{2u} mode could be due to the decrease in the lattice parameter by replacing O with N and might be due to the strong screening effects in La_3InN. Altogether the hardening of the phonon modes in the presence of the Z (Z=N, O) atom in the body centered position of the cube plays a role in decreasing the electron–phonon coupling constant eventually leading to the lower T_c in La_3InZ as compared to La_3In.

4. Conclusion

In summary, our ab initio study of electronic structure calculation of La_3InZ (Z=N, O) conclude that, when the Z atom is added to the body center of the La_3In, the hybridizing effect between La-*d* and In-*p* orbital gets reduced in La_3InZ in comparison with La_3In. The Fermi surface topology change is observed under compression for La_3InO but not in La_3InN, which is attributed to the non-monotonic variation of the density of states in La_3InO. From the phonon dispersion plots we have shown both the compounds to be dynamically stable. Analysis of the superconductivity of the La_3InZ shows the suppression of T_c in addition of the Z (N, O) atom in La_3In, which is mainly due to the hardening of the phonon modes due to the presence of the Z atom and is confirmed from the phonon density of states. From our calculated superconductivity we find the T_c to be less than 2 K for N containing compound, whereas T_c is calculated above 2 K for O containing compound and also well support the experimental trend.

Acknowledgments

The authors would like to acknowledge IIT Hyderabad for providing the computational facility. S.R. acknowledges MHRD for the fellowship.

References

[1] F. Heiniger, E. Bucher, J.P. Maita, P. Descouts, Phys. Rev. B 8 (1973) 3194–3205.
[2] R. Nagarajan, Chandan Mazumdar, Zakir Hossain, S.K. Dhar, K.V. Gopalakrishnan, L.C. Gupta, C. Godart, B.D. Padalia, R. Vijayaraghavan, Phys. Rev. Lett. 72 (1994) 274.
[3] P. Ravindran, R. Asokamani, J. Phys.: Condens. Matter 7 (1995) 5567.
[4] D. Jung, Bull. Korean Chem. Soc. 20 (1999) 281.
[5] W. Mickelson, J. Cumings, W.Q. Han, A. Zettl, Phys. Rev. B 65 (2002) 052505.
[6] Jing-Tai Zhao, Zhen-Chao Dong, J.T. Vaughey, Jerome E. Ostenson, D. John Corbett, J. Alloys Compd. 230 (1995) 1–12.
[7] M. Kirchner, W. Schnelle, F.R. Wagner, R. Niewa, Solid State Sci. 5 (2003) 1247–1257.
[8] P. Blaha, K. Schwarz, G.K.H. Madsen, D. Kvasnicka, J. Luitz, WIEN2K, An Augmented Plane Wave + Local Orbitals Program for Calculating Crystal Properties, Karlheinz Schwarz, Techn. Universität, Wien, Austria, 2001.
[9] J.P. Perdew, K. Burke, M. Ernzerhof, Phys. Rev. Lett. 77 (1996) 3865.
[10] H.J. Monkhorst, J.D. Pack, Phys. Rev. B 13 (1976) 5188.
[11] A. Kokalj, Comput. Mater. Sci. 28 (2003) 155.
[12] P. Giannozzi, S. Baroni, N. Bonini, M. Calandra, R. Car, C. Cavazzoni, D. Ceresoli, G.L. Chiarotti, M. Cococcioni, I. Dabo, et al., J. Phys.: Condens. Matter 21 (2009) 395502.
[13] S. Baroni, S. de Gironcoli, A. Dal Corso, P. Giannozzi, Rev. Mod. Phys. 73 (2001) 515.

[14] Swetarekha Ram, V. Kanchana, A. Svane, S.B. Dugdale, N.E. Christensen, communicated.
[15] Swetarekha Ram, V. Kanchana, A. Svane, S.B. Dugdale, N.E. Christensen, in preparation.
[16] Swetarekha Ram, V. Kanchana, A. Svane, S.B. Dugdale, N.E. Christensen, J. Phys.: Condens. Matter 25 (2013) 155501.
[17] P.B. Allen, R.C. Dynes, J. Phys. C: Solid State Phys. 8 (1975) L158.
[18] S.A. Ostanin, V.Yu. Trubitsin, S.Yu. Savrasov, M. Alouani, H. Dreyssé, Comput. Mater. Sci. 17 (2000) 202.
[19] R.A. Jishi, H.M. Alyahyaei, Adv. Condens. Matter Phys. 2010 (2010) 6.